Vietnam Journal of Mechanics, VAST, Vol. 37, No. 4 (2015), pp. 239 – 250
DOI:10.15625/0866-7136/37/4/5918

FAILURE MECHANISM OF TWO-DIMENSIONAL GRANULAR COLUMNS: NUMERICAL SIMULATION AND EXPERIMENTS

Nguyen Tien Cuong[1,3,*], **Bui Hong Ha**[2], **Ryoichi Fukagawa**[3]
[1]*Institute of Mechanics, Vietnam Academy of Science and Technology, Hanoi, Vietnam*
[2]*Monash University, Melbourne, Australia*
[3]*Ritsumeikan University, Kusatsu, Japan*
[*]E-mail: ntcuong@imech.ac.vn
Received January 22, 2015

Abstract. In this article, two typical experiments for two types of destruction of granular column were performed by 2D soil model. High speed camera was used to record the movements of the destruction of the granular column. The images clearly showed the whole development of granular flows. The destruction process of the granular column in the two experiments is a big deformation problem of soil mechanics. To simulate the destruction process of the granular column, a model solving the problem of soil mechanics by Smoothed Particle Hydrodynamics (SPH) method was developed. The basic equations of problems of soil mechanics using the Drucker-Prager constitutive model were discretized using SPH method. The calculation results of the numerical model developed by us were compared with the experiment results obtained at the same time since the destruction of the granular column started. This was the first time by comparing and analyzing in details the characteristics of the process of destruction and developments of granular flows for the two typical types of destruction of granular column, it was shown that the numerical model describes quite accurately the characteristics of granular flows in both space and time.

Keywords: Granular flow, failure mechanism of granular column, 2D soil experiment, SPH method, mesh-free particle method.

1. INTRODUCTION

In recent years, the landslides caused by earthquakes and landslides caused by storm rains with high intensity for a long time have been increasing, especially in countries with frequent earthquakes like Japan and the countries with dangerous mountainous terrain and impacts of global climate change, such as Vietnam, Philippines and Indonesia. Landslide has threatened the safety of lives and properties of the people living in the steep mountainous areas with easily destructed geological structure.

To limit the damages to humans and properties due to natural disasters, the prevention work by early warning and predicting landslides as well as evacuating the people away from the areas with high risks of landslides is essential. To delineate areas with high risk of landslide, as well as forecast, warn landslides besides studies of geological survey, numerical models are necessary for simulation, calculation of erosion thresholds and conditions.

Since 2004, many authors and researcher groups have studied this problem both experimentally and theoretically with the aim to find out the characteristics of the process such as destroyed domain, areas affected by destruction,... These characteristics are of great significance in the planning of residential development in areas with high risk of landslide. The authors who used experiments to study this problem include Lube et al. [1,2], Balmforth et al. [3], Lajeunesse et al. [4,5]), Trepanier et al. [6], Warnett et al. [7], Nguyen et al. [8]... In addition to the researcher groups based on experiments, a lot of authors and researcher groups studied the theory and the numerical model simulate this problem such as Staron et al. [9], Bui [10], Bui et al. [11, 12]), Blanc [13], Artoni et al. [14], Kumar et al. [15], Midi et al. [16]. The numerical models which were developed to study the erosion problem could be classified into two types, mesh-based models (such as finite element method, finite difference method) and mesh-free methods... The mesh-based method allows to predict the landslide thresholds and conditions and sliding limit but cannot describe the landslide process and forecast the state after the landslide. The mesh-free method overcomes the above disadvantages which the mesh-based methods fail to do. The whole landslide process and state after landslide can be calculated and simulated. The mesh-free methods are used to study this problem, mainly the Discrete Element Method (DEM) method and Smoothed Particle Hydrodynamics (SPH) method.

The typical researcher group who applied the DEM method may include Staron et al. [9], Kumar et al. [15], Crosta et al. [17], Bui et al. [11,12]) and Utili et al. [18]. In 2008, Bui et al. [11] was one of the researcher groups leading in the application of SPH method to solve this problem, later there were many more researcher groups who applied SPH method to study this problem such as Blanc [13], Midi et al. [16]. So far the publications related to the application of SPH method to study 2D-soil granular flows have just stopped at the verification of calculation results of the models with experiment results at the last moment, i.e. when the destruction of the granular column ended. In this article, it is the first that the results of the 2D granular flow problem model using SPH method have been fully verified with experiments in both space and time.

2. MATHEMATICAL FORMULATION AND NUMERICAL METHOD

2.1. SPH meshfree particle method

The SPH method was independently developed by two group authors (Lucy [19]; R. A. Gingold and J. J. Monaghan [20]) for astrophysics applications. Since its invention, the SPH method has been extended to various applications such as fluid mechanics (Monaghan [21]), solid mechanics (Libersky et al. [22]) and geomechanics (Bui et al. [11,12]).

SPH methods include two essential formulas for a function and the derivative of a function such as Eqs. (1) and (2) below.

$$\begin{aligned} A(r) &= \int A(r')W(|r-r'|,h)dr' + O(h^2) \\ &= \int \frac{A(r')}{\rho(r')}W(|r-r'|,h)\rho(r')dr' + O(h^2) \\ &\approx \sum_{b=1}^{N} \frac{m_b}{\rho_b} A_b W\left(|r-r_b|,h\right), \end{aligned} \tag{1}$$

$$\begin{aligned} \nabla A(r) &= \frac{\partial}{\partial r}\int \frac{A(r')}{\rho(r')}W(|r-r'|,h)\rho(r')dr' + O(h^2) \\ &\approx \sum_{b=1}^{N} m_b \frac{A_b}{\rho_b}\nabla_a W_{ab}\ , \end{aligned} \tag{2}$$

where A - any variable defined on the spatial coordinate r; W - kernel function which is chosen to be the cubic-spline function; and h - smoothing length which specifies the interpolation area; m - mass of particle; b - the quantity evaluated at the position of particle b and

$$\nabla_a W_{ab} \equiv \frac{r_{ab}}{|r_{ab}|}\frac{\partial W_{ab}}{\partial r_a}. \tag{3}$$

2.2. Motions of granular flows in SPH

The basic equations used to describe the motion of soil in the SPH framework are the continuity equation and the momentum equation (Bui et al. [11]). These two equations are written as follows

$$\frac{d\rho}{dt} = -\frac{1}{\rho}\nabla.v\ , \tag{4}$$

$$\rho\frac{dv}{dt} = \nabla.\sigma + \rho g + f_{ext}\ , \tag{5}$$

where v is the vector velocity of soil particle; ρ is the density; σ is the total stress tensor, taken negative for compression; g is the acceleration due to gravity; and f_{ext} is additional external forces. The total stress tensor of soil is normally composed of the effective stress (σ') and the pore-water pressure (p_w), which followed the Terzaghi's concept of effective stress. Because the pore-water pressure is not considered, the total stress tensor and the effective stress are identical throughout this paper and can be computed using any material constitutive model.

Applying Eq. (2), the partial differential form of equations Eqs. (4) and (5) can be discretized in the SPH framework in the following way (Bui et al. [11])

$$\frac{d\rho_a}{dt} = \sum_{b=1}^{N} m_b\left(v_a^{\alpha} - v_b^{\alpha}\right)\frac{\partial W_{ab}}{\partial x_a^{\alpha}}\ , \tag{6}$$

$$\frac{dv_a^{\alpha}}{dt} = \sum_{b=1}^{N} m_b\left(\frac{\sigma_a^{\alpha\beta}}{\rho_a^2} + \frac{\sigma_b^{\alpha\beta}}{\rho_b^2} + C_{ab}^{\alpha\beta}\right)\frac{\partial W_{ab}}{\partial x_a^{\beta}}\nabla + g_a^{\alpha} + f_{ext\to a}^{\alpha}\ , \tag{7}$$

where α and β denote Cartesian components x, y, z with the Einstein convention applied to repeated indices; a indicates the particle under consideration; ρ_a and ρ_b are the densities of particle a and b respectively; N is the number of "neighboring particles", i.e. those in the support domain of particle a; m_b is the mass of particle b; $C_{ab}^{\alpha\beta}$ is the stabilization term employed to remove the stress fluctuation and tensile instability (Bui et al. [12]); and $f_{ext\to a}$ is the external force acting on particle a.

The stress tensor in Eq. (7) can be computed using any soil constitutive model developed in the literature, which are applicable for the finite element method (FEM). In this paper, the Drucker-Prager constitutive model with non-associated flow rule was chosen. This model was implemented in the SPH framework by Bui et al. [11], and was shown to be an appropriate soil model for simulating large deformation and post-failure behavior of aluminum rods which are used in the current paper as model ground. The stress-strain relation of this soil model is given by

$$\dot{\sigma} = D^e : (\dot{\varepsilon} - \dot{\varepsilon}^p) \ , \tag{8}$$

where D^e is the elastic constitutive tensor; $\dot{\varepsilon}^p$ is the strain rate tensor; and is its plastic component. Here, an additive decomposition of the strain rate tensor has been assumed into elastic and plastic components. The plastic component can be calculated using the plastic flow rule

$$\dot{\varepsilon}^p = \dot{\lambda} \frac{\partial g_p}{\partial \sigma} \ , \tag{9}$$

where $\dot{\lambda}$ is the rate of change of plastic multiplier, and g_p is the plastic potential function. The plastic deformation occurs only if the stress state reaches the yield surface. Accordingly, plastic deformation will occur only if the following yield criterion is satisfied

$$f = \alpha_\phi I_1 + \sqrt{J_2} - k_c = 0 \ , \tag{10}$$

where I_1 and J_2 are the first and second invariants of the stress tensor; and a_ϕ and k_c are Drucker-Prager constants that are calculated from the Coulomb material constants c (cohesion) and ϕ (internal friction). In plane strain, the Drucker-Prager constants are computed by

$$\alpha_\phi = \frac{\tan\phi}{\sqrt{9 + 12\tan^2\phi}} \ , \tag{11}$$

and

$$k_c = \frac{3c}{\sqrt{9 + 12\tan^2\phi}} \ . \tag{12}$$

The non-associated plastic flow rule specifies the plastic potential function by

$$g_p = \alpha_\psi I_1 + \sqrt{J_2} - \text{const} \ , \tag{13}$$

where α_ψ is a dilatancy factor that can be related to the dilatancy angle ψ in a fashion similar to that between α_ϕ and friction angle ϕ. Substituting Eq. (9) into Eq. (8) in association with the consistency condition, that is the stress state must be always located on the yield

surface f during the plastic loading, the stress-strain relation of the current soil model at particle a can be written as

$$\frac{d\sigma_a^{\alpha\beta}}{dt} = 2G_a\dot{e}_a^{\alpha\beta} + K_a\dot{\varepsilon}_a^{\gamma\gamma}\delta_a^{\alpha\beta} - \dot{\lambda}_a\left[3K_a\alpha_{\psi a}\delta^{\alpha\beta} + \left(\frac{G}{\sqrt{J_2}}\right)_a s_a^{\alpha\beta}\right] , \tag{14}$$

where $\dot{e}_a^{\alpha\beta} = \dot{\varepsilon}_a^{\alpha\beta} - \frac{1}{3}\dot{\varepsilon}_a^{\gamma\gamma}\delta^{\alpha\beta}$ is the deviatoric strain-rate tensor; $s^{\alpha\beta}$ is the deviatoric shear stress tensor; and $\dot{\lambda}_a$ is the rate of change of plastic multiplier of particle a, which in SPH is specified by

$$\dot{\lambda}_a = \frac{3\alpha_{\phi a}K_a\dot{\varepsilon}_a^{\gamma\gamma} + \left(G/\sqrt{J_2}\right)_a s_a^{\alpha\beta}\dot{\varepsilon}_a^{\alpha\beta}}{9\alpha_{\phi a}K_a\alpha_a + G_a} , \tag{15}$$

and $\dot{\varepsilon}_a^{\alpha\beta}$ is the strain-rate tensor computed by

$$\dot{\varepsilon}_a^{\alpha\beta} = \frac{1}{2}\sum_{b=1}^{N}\frac{m_b}{\rho_b}\left(v_b^\alpha - v_a^\alpha\right)\frac{\partial W_{ab}}{\partial x_a^\beta} + \frac{1}{2}\sum_{b=1}^{N}\frac{m_b}{\rho_b}\left(v_b^\beta - v_a^\beta\right)\frac{\partial W_{ab}}{\partial x_a^\alpha} . \tag{16}$$

When considering a large deformation problem, a stress rate that is invariant with respect to rigid-body rotation must be employed for the constitutive relations. In the current study, the Jaumann stress rate, $\hat{\sigma}_a^{\alpha\beta}$ is adopted

$$\hat{\sigma}_a^{\alpha\beta} = \dot{\sigma}_a^{\alpha\beta} - \sigma_a^{\alpha\gamma}\dot{\omega}_a^{\beta\gamma} - \sigma_a^{\gamma\beta}\dot{\omega}_a^{\alpha\gamma} , \tag{17}$$

where $\dot{\omega}_a^{\alpha\beta}$ is spin-rate tensor computed by

$$\dot{\omega}_a^{\alpha\beta} = \frac{1}{2}\sum_{b=1}^{N}\frac{m_b}{\rho_b}\left(v_b^\alpha - v_a^\alpha\right)\frac{\partial W_{ab}}{\partial x_a^\beta} - \frac{1}{2}\sum_{b=1}^{N}\frac{m_b}{\rho_b}\left(v_b^\beta - v_a^\beta\right)\frac{\partial W_{ab}}{\partial x_a^\alpha} . \tag{18}$$

As a result, the final form of the stress-strain relationship for the current soil model is modified to

$$\frac{d\sigma_a^{\alpha\beta}}{dt} = \sigma_a^{\alpha\beta}\dot{\omega}_a^{\beta\gamma} + \sigma_a^{\gamma\beta}\dot{\omega}_a^{\alpha\gamma} + 2G_a\dot{e}_a^{\alpha\beta} + K_a\dot{\varepsilon}_a^{\gamma\gamma}\delta_a^{\alpha\beta} - \dot{\lambda}_a\left[3K_a\alpha_{\psi a}\delta^{\alpha\beta} + \left(\frac{G_a}{\sqrt{J_{2a}}}\right)s_a^{\alpha\beta}\right] . \tag{19}$$

The above soil constitutive model requires six soil parameters: cohesion (c), friction angle (ϕ), dilatancy angle (ψ), Young's modulus (E), Poisson's ratio (υ), and soil density (ρ).

3. EXPERIMENTAL

2D granular column experiments were performed with a 2D soil model created by aluminum bars with a diameter of 3 mm and 2 mm at the ratio of 2:3. The 2D soil model created had the properties as shown in Tab. 1.

The experiment was designed as in Fig. 1. In the figure, the axis $0x$ and $0y$ are hard edges. Soil blocks are bounded at the bottom by $0x$, the left by $0y$ and the right by shield. The right shield will be removed rapidly during the experiment. In Fig. 1, h_0 and d_0 are respectively the original height and width of the granular column. The experiment was

Table 1. Soil properties

Name	Value	Unit
Density (ρ)	2074	(Kg/m^3)
Friction angle (ϕ)	21.9	(deg)
Young's module (E)	5.84	(Mpa)
Poisson's ratio (v)	0.3	
Dilatant angle (ψ)	0	(deg)
Cohesion (c)	0	(kPa)

carried out in two options characterizing the destruction types of granular flow corresponding to the following parameters: Option 1: $h_0 = 10$ (cm), $d_0 = 20$ (cm); Option 2: $h_0 = 10$ (cm), $d_0 = 10$ (cm).

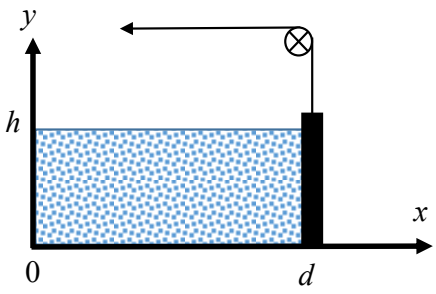

Fig. 1. Experiment model

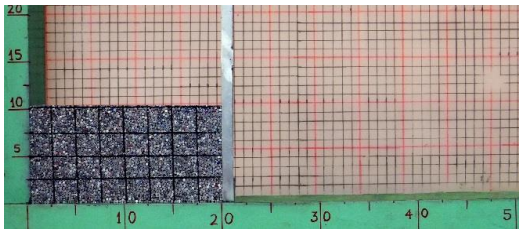

Fig. 2. Experiment setup

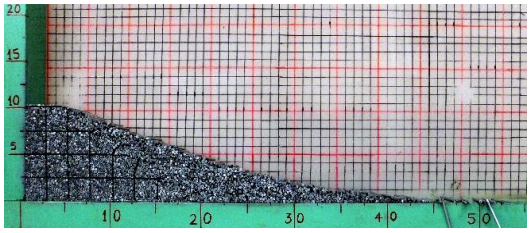

Fig. 3. Final result of experiment

Initially, the experiment was setup as shown in Fig. 2. After the right shield of the soil block was removed, the granular column would be destroyed. The destruction process of the granular column was recorded by Photron high speed camera to test the numerical model in both mechanism and time of the granular column destruction. The experiment results in Fig. 3 is a picture after the destruction of the granular column ends.

4. RESULTS AND COMPARISONS

The numerical model is established to calculate and simulate the 2D granular flow problem with the size parameters of the granular column and the properties of the 2D soil

model as described in Tab. 1 and Fig. 1 above. To get the overall picture of the destruction mechanism of the granular column, this study calculated and compared the two cases representing two types of destruction of the granular column with experimental data corresponding to the value of the ratio $a = h_0/d_0$ of the domains $a > 0.65$ and $a < 0.65$.

4.1. Option 1

The calculation option has $h_0 = 10$ (cm), $d_0 = 20$ (cm) and $a = 0.5 < 0.65$. With such parameters of the granular column, after the destruction of the granular column ended, the height of remaining granular column was still equal to the initial height of the granular column of 10 (cm). The calculation results of the destruction process of the granular column were compared with the experiment results obtained at the same time as shown in Fig. 4.

Fig. 4b shows that the calculation results and experiment results at the time 0.09 (s). Fig. 4b shows that the calculation results and experiment results are basically the same. The difference at this time is the development process at the base of the shape of the granular flow in the early stage of the collapse of the granular column in the experiment results.

The calculation and experiment results at the time of 0.13 (s) as in Fig. 4c. At this time, the impact of the movement on the right shield is no longer available, so the calculation and experiment results are very similar both qualitatively and quantitatively. The base of the granular flow at this time, according to the calculation results, has spread to the position 27.0 (cm), whereas the experiment results are 26.5 (cm). The destroyed domain the top of the granular column, as calculated and experimented, is 7.6 (cm) and 8.4 (cm), respectively.

Fig. 4d compares the calculation results and the experiment results at 0.17 (s). If at 0.13 (s), the surface of granular flow has convex bow shape as in Fig. 4c. At this point, the shape of granular flow surface starts to turn into concave form and appeared intermittent on the surface, making the granular flow surface at the base and the peak have two different corners. At this time, the simulation and experiment results show that the granular flow has reached the position 31.0 (cm). The destroyed domain the top of the granular column, as calculated and experimented, is 7.5 (cm) and 8.4 (cm), respectively.

At $t = 0.21$ (s), the intermittent point is shown clearly as in Fig. 4e. At this time, the surface of the granular flow forms two straight lines coming from the base and the peak of the granular flow and intersecting at the intermittent point as in Fig. 4d. These two lines made the granular flow surface have different peak and bottom corners. The simulation and experiment results clearly show this phenomenon. At this time, according to the simulation, the granular flow has reached the position 36 (cm), and according to experiment, it is 35.5 (cm). The starting point of the destroyed domain on the top of the granular column, as calculated and experimented, is 7.0 (cm) and 8.1 (cm), respectively.

At the time $t = 0.27$ (s), the intermittent point is no longer available, the surface of the granular flow is shaped like a smooth concave curve as shown in Fig. 4f. The difference between the base and top corners of the granular flow is gradually contracted. The simulation and experiment results clearly show that the granular flow has reached the position 41 (cm). The starting point of the destroyed domain on the top of the granular

column, as calculated and experimented, is 6.5 (cm) and 7.7 (cm), respectively. Fig. 4f also shows the calculation results are very similar to the experiment results in both granular flow surface structure and the destroyed domain shape and run out distance.

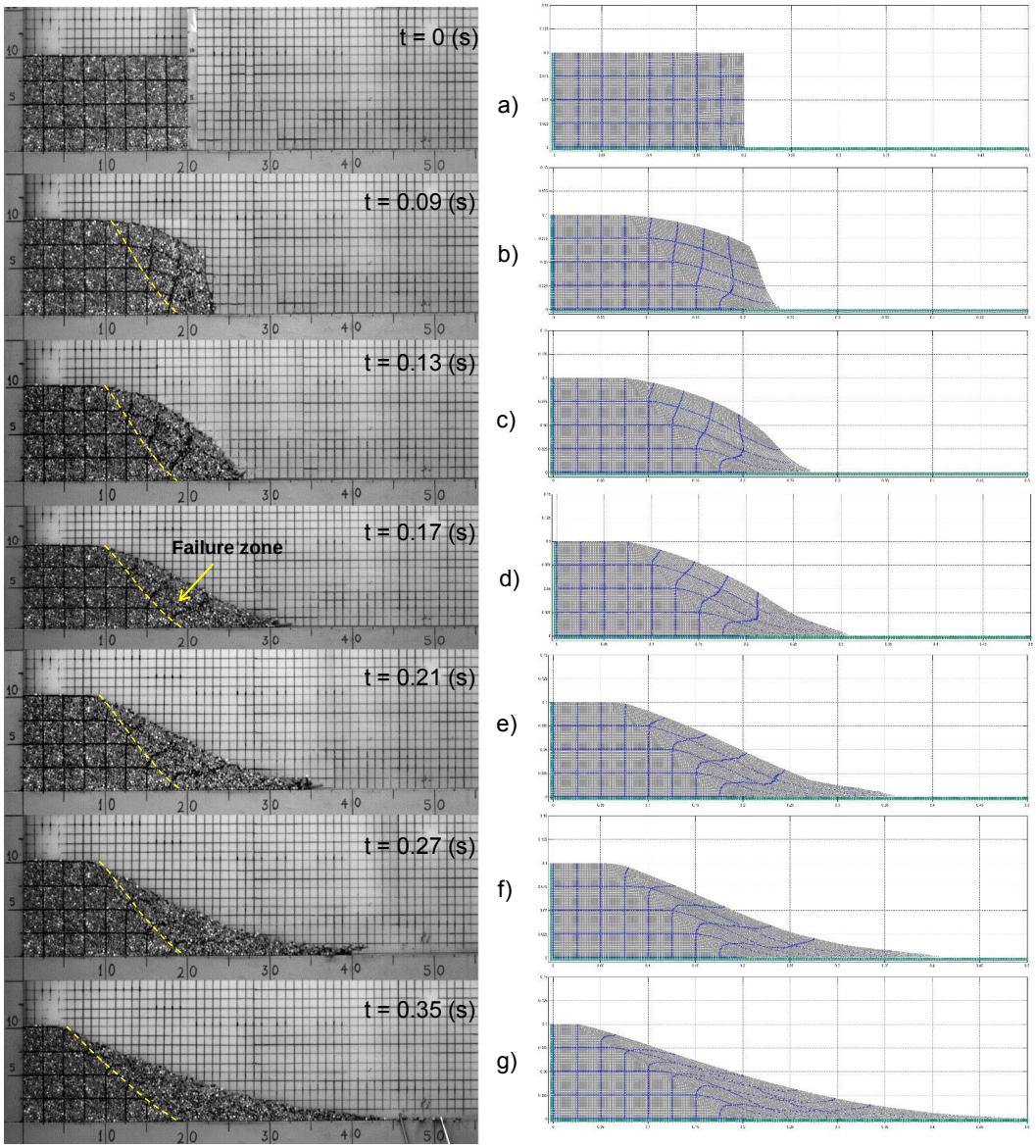

Fig. 4. Comparison between experimental result and numerical simulation result ($h_0 = 10, d_0 = 20$)

Towards the end of the destruction process of the granular column, the granular flow surface tends to reduce the curvature and the two corners at the base and top of the granular flow approach each other and close to the corner of internal friction of the

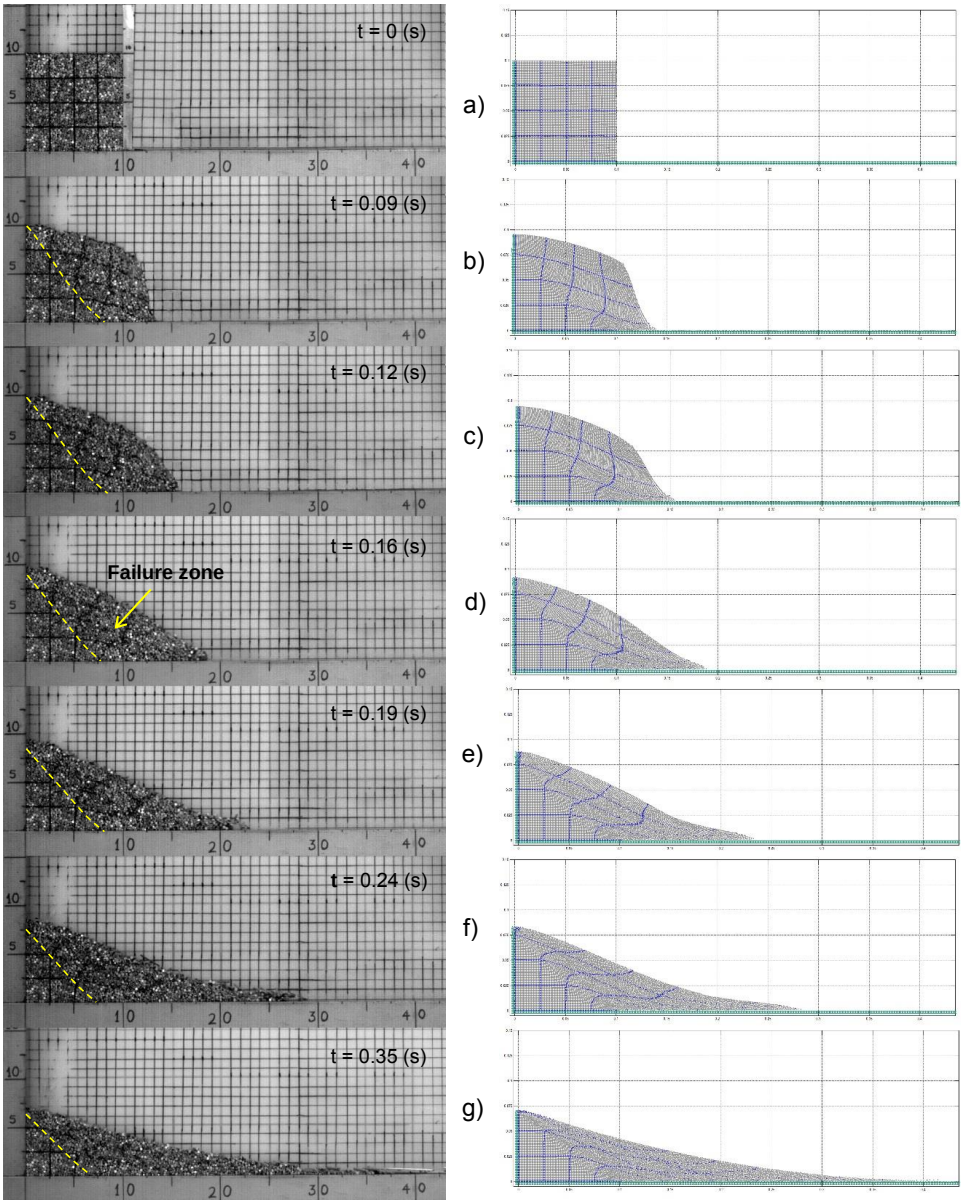

Fig. 5. Comparison between experimental result and numerical simulation result ($h_0 = 10, d_0 = 10$)

material. The calculation and experiment results at the end of the destruction process of the granular flow is shown in Fig. 4g. The comparison of characteristics such as the shape of granular flow surface, form and parameters of the destroyed domain and the material run out distance between the simulation results and experiment results as shown

in Fig. 4g shows that the calculation results correctly and accurately reflect compared with experiment results.

4.2. Option 2

The calculation option has $h_0 = 10$ (cm), $d_0 = 10$ (cm) and $a = 1.0 > 0.65$. With such parameters of the granular column, after the destruction of the granular column ended, the height of remaining granular column was less than the initial height of the granular column. The calculation results of the destruction process of the granular column were compared with the experiment results obtained at the same time as shown in Fig. 5.

The calculation results are compared to the experiment results at $t = 0.09$ (s) as in Fig. 5b, $t = 0.12$ (s) as in Fig. 5c, $t = 0.16$ (s) as in Fig. 5d, $t = 0.19$ (s) as in Fig. 5e, $t = 0.24$ (s) as in Fig. 5f and the final results of the destruction process of the granular column as shown in Fig. 5g. Fig. 5 shows the calculation results and experiment results are very similar in terms of the variation of the transient surface of the granular flow, the variation of the destroyed domain as well as the run out distance of the granular flow.

Unlike Option 1, in this option, the ratio $a > 0.65$, so the height of the remaining granular column after the destruction h is smaller than the initial height h_0 of the granular column, i.e. $h < h_0$. The calculation results also show that the value of granular column height h at the time of comparison is always very close to the value observed in the experiment results.

5. CONCLUSIONS

The images recorded with high speed camera comprehensively and completely show both space and time of the destruction of the two granular columns. These are the experimental data with sufficient information to allow other authors to use to verify the numerical models or refer to and compare with their experiment results.

Through the comparison of the simulation results of the numerical model developed by us with the experiment results for the two types of destruction of the granular column, it was obtained that the calculation results of the numerical model not only accurately reflect the geometric parameters of the destruction of the granular column (such as the shape of granular flow surface, destroyed domain, run out distance) but also show that the times of the destruction landmarks of the granular column between calculation and experiment are identical. The previously publications only compared the calculation results with the experiment results at the end of the destruction process, but not mentioned the entire destruction process as well as the time aspect. This article shows the overall picture in both time and space of the destruction process of the granular flow, and our numerical model has properly described those elements. Verifying the calculation results with the experiment results in both spatial and time characteristics of the destruction demonstrates the great advantage of the numerical model.

The findings in this article show that the numerical model solving the problem of soil mechanics by the mesh-free method SPH developed by us has high accuracy. With the outstanding features of the mesh-free method SPH, compared to conventional mesh-based methods, which allows calculation and simulation of big deformation problems,

the calculation model developed by us has enough capacity and reliability to calculate and simulate the landslide problem to serve the design of building of anti-erosion or landslide prediction and warning.

ACKNOWLEDGEMENTS

The first author would like to thank JSPS (Japan Society for the Promotion of Science) for their financial supports by RONPAKU fellowship ID number VNM11010.

REFERENCES

[1] G. Lube, H. E. Huppert, R. S. J. Sparks, and M. A. Hallworth. Axisymmetric collapses of granular columns. *Journal of Fluid Mechanics*, **508**, (2004), pp. 175–199.

[2] G. Lube, H. E. Huppert, R. S. J. Sparks, and A. Freundt. Collapses of two-dimensional granular columns. *Physical Review E*, **72**, (4), (2005), pp. 1–10. Doi: 10.1103/PhysRevE.72.041301.

[3] N. J. Balmforth and R. R. Kerswell. Granular collapse in two dimensions. *Journal of Fluid Mechanics*, **538**, (2005), pp. 399–428.

[4] E. Lajeunesse, A. Mangeney-Castelnau, and J. P. Vilotte. Spreading of a granular mass on a horizontal plane. *Physics of Fluids*, **16**, (7), (2004), pp. 2371–2381.

[5] E. Lajeunesse, J. B. Monnier, and G. M. Homsy. Granular slumping on a horizontal surface. *Physics of Fluids*, **17**, (10), (2005). Doi: 10.1063/1.2087687.

[6] M. Trepanier and S. V. Franklin. Column collapse of granular rods. *Physical Review E*, **82**, (1), (2010). Doi: 10.1103/PhysRevE.82.011308.

[7] J. M. Warnett, P. Denissenko, P. J. Thomas, E. Kiraci, and M. A. Williams. Scalings of axisymmetric granular column collapse. *Granular Matter*, **16**, (1), (2014), pp. 115–124.

[8] C. T. Nguyen, H. H. Bui, and R. Fukagawa. Failure mechanism of true 2D granular flows. *Journal of Chemical Engineering of Japan*, **48**, (6), (2015), pp. 1–8.

[9] L. Staron and E. J. Hinch. Study of the collapse of granular columns using two-dimensional discrete-grain simulation. *Journal of Fluid Mechanics*, **545**, (2005), pp. 1–27.

[10] H. H. Bui. *Lagrangian mesh-free particle method (SPH) for large deformation and post-failure of geomaterials using elasto-plastic soil constitutive models*. PhD thesis, Ritsumeikan University, Japan, (2007).

[11] H. H. Bui, R. Fukagawa, K. Sako, and S. Ohno. Lagrangian meshfree particles method (SPH) for large deformation and failure flows of geomaterial using elastic-plastic soil constitutive model. *International Journal for Numerical and Analytical Methods in Geomechanics*, **32**, (12), (2008), pp. 1537–1570.

[12] H. H. Bui, R. Fukagawa, K. Sako, and J. C. Wells. Slope stability analysis and discontinuous slope failure simulation by elasto-plastic smoothed particle hydrodynamics (SPH). *Geotechnique*, **61**, (7), (2011), pp. 565–574.

[13] T. Blanc. *Numerical simulation of debris flows with the 2D-SPH depth integrated model*. PhD thesis, (2008).

[14] R. Artoni, A. C. Santomaso, F. Gabrieli, D. Tono, and S. Cola. Collapse of quasi-two-dimensional wet granular columns. *Physical Review E*, **87**, (3), (2013). DOI: 10.1103/PhysRevE.87.032205.

[15] K. Kumar, K. Soga, and J.-Y. Delenne. Multi-scale modelling of granular avalanches. In *AIP Conference Proceedings*, Vol. 1542, (2013), pp. 1250–1253.

[16] G. D. R. Midi. On dense granular flows. *The European Physical Journal E*, **14**, (4), (2004), pp. 341–365.

[17] G. B. Crosta, S. Imposimato, and D. Roddeman. Numerical modeling of 2-D granular step collapse on erodible and nonerodible surface. *Journal of Geophysical Research: Earth Surface (2003–2012)*, **114**, (F3), (2009). DOI: 10.1029/2008JF001186.

[18] S. Utili, T. Zhao, and G. T. Houlsby. 3D DEM investigation of granular column collapse: Evaluation of debris motion and its destructive power. *Engineering Geology*, **186**, (2015), pp. 3–16.

[19] L. B. Lucy. A numerical approach to the testing of the fission hypothesis. *The Astronomical Journal*, **82**, (1977), pp. 1013–1024.

[20] R. A. Gingold and J. J. Monaghan. Smoothed particle hydrodynamics: Theory and application to non-spherical stars. *Monthly Notices of the Royal Astronomical Society*, **181**, (3), (1977), pp. 375–389.

[21] J. J. Monaghan. Simulating free surface flows with SPH. *Journal of Computational Physics*, **110**, (2), (1994), pp. 399–406.

[22] L. D. Libersky, A. G. Petschek, T. C. Carney, J. R. Hipp, and F. A. Allahdadi. High strain lagrangian hydrodynamics: a three dimensional SPH code for dynamic material response. *Journal of Computational Physics*, **109**, (1993), pp. 67–75.